0163–4984/96/3602–3–0135 $13.00

Synthesis of Nanoscale Magnetic Metal Particles Encapsulated in Magnesium Fluoride and the Properties of These Materials

DAJIE ZHANG,[1] KENNETH J. KLABUNDE,*[,1]
CHRISTOPHER M. SORENSEN,[1]
AND GEORGE C. HADJIPANAYIS[2]

Departments of Chemistry and Physics, Kansas State University, Manhattan, KS; and Department of Physics, University of Delaware, Newark, DE

Accepted January 20, 1997

ABSTRACT

Core-shell Fe-MgF_2, Co-MgF_2, nanocomposites were prepared by the Solvated-Metal-Atom-Dispersion (SMAD) method. X-ray powder diffraction (XRD), transmission electron microscopy (TEM), and superconducting quantum interference device (SQUID) magnetometry were used to elucidate the thermal and oxidative behaviors and the magnetic properties of these materials. The Fe-MgF_2, Co-MgF_2, and Ni-MgF_2 particles heat-treated at temperatures below 350°C had reduced magnetization 40–60% below their bulk values after these materials were exposed to air. However, if instead the particles were heat-treated at higher temperatures followed by oxidative passivation, they exhibited corrected magnetization values close to their bulk values. The magnetization data together with the XRD and TEM studies proved that the Fe, Co, and Ni crystallites were well protected by the MgF_2 shell. Studies on the Fe-BaF_2 combination are also reported.

Index Entries: Magnetic particles; nanoscale; encapsulated; iron; magnesium fluoride.

INTRODUCTION

Nanometer-sized metallic particles, such as Fe, Co, and Ni, have been attracting more and more attention in the development of new magnetic

*Author to whom all correspondence and reprint requests should be addressed.

recording materials *(1–3)*. Since these metal particles are very sensitive to oxygen, a big challenge is to prevent them from oxidation. A protecting matrix is needed in order to encapsulate the metal particles, so they can be handled in air. Otherwise, their applications will be severely limited. The protecting reagent for this purpose can be a metal, as studied before *(4–6)*. It can also be a solid-state molecular compound or a polymer. Indeed, metal nanoparticles embedded in such solid matrices represent an important new class of composite materials. The most-studied metal-insulator system in the field of nanometer-sized magnetic clusters is the Fe-SiO_2 system, and is often referred to as Fe-SiO_2 granular solids, which are prepared either by coevaporation/codeposition of SiO_2 and Fe *(7,8)*, or by high-energy ball milling *(9)*. Other known Fe-based nanocomposite materials include Fe-$A1_2O_3$ *(10)*, Fe-MgO *(11)*, and Fe-NaY zeolite *(12)*. The nonmagnetic, nonconducting matrix in these Fe-based nanocomposite materials not only serves as a stable host for the small Fe clusters, but may also have a significant impact on the microstructure-related magnetic properties of the ferromagnetic particles. These properties include the surface magnetic moment, coercivity, and Mössbauer parameters. Unlike the naturally formed oxide coating on these small ferromagnetic particles, such as Fe_2O_3 and Fe_3O_4, these host materials are nonmagnetic. This enables one to rule out magnetic interactions between the host material and the magnetic particles, and therefore perhaps more straightforward data interpretation.

Herein we report an additional method to prepare such composites with the particular advantage that fine powders are produced instead of films. This is done by using the Solvated-Metal-Atom-Dispersion (SMAD) technique *(13a–c)*. This method involves the codeposition of the host shell material (e.g., MgF_2 vapor) with metal vapor, with the simultaneous deposition at 77 K of an excess of a hydrocarbon diluent (solvent). After deposition and slight warming above 77 K, kinetic growth of MgF_2-metal particles takes place. The metastable particles are isolated and heat-treated to cause phase segregation, hopefully into core-shell particles (Scheme 1).

The requirements for a successful preparation are that the shell material be inert toward the metal atoms and growing clusters, and be capable of protecting the encapsulated metal clusters from air oxidation.

EXPERIMENTAL APPROACH

Chemicals

Iron metal, chips, 99.98%, Aldrich Chemical Co., Inc. (Milwaukee, WI);
Cobalt, pieces, 99.5%, Aldrich Chemical Co. Inc.;
Nickel, shot, Assay(Ni) 100.6%, J.T. Baker Chemical Co. (Phillipsburg, NJ);
MgF_2, pieces, 3–6 mm, 99.9%, Aldrich Chemical Co.;

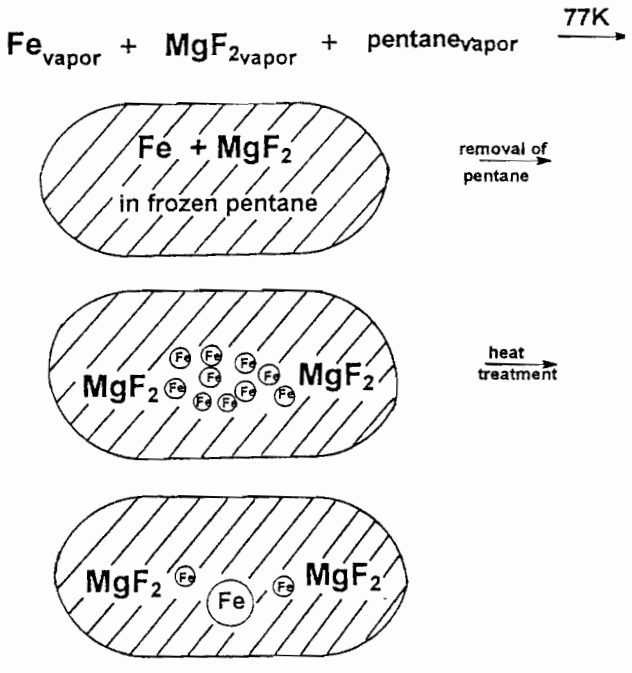

Scheme 1. Encapsulation of Fe clusters in MgF_2.

Barium fluoride, random crystals, 99.999%, optical-grade, Aldrich Chemical.; and
n-Pentane, HPLC-grade, Fisher Chemical/Fisher Scientific (Burr Ridge, IL).

The pentane used was predried by refluxing over Na/K with benzopheone. Before going to the SMAD reactor, the dried pentane held in a Schlenk tube was degassed on a vacuum line with liquid nitrogen. The crucibles used for metal evaporation were tungsten baskets obtained from R. D. Mathis Company; they were coated with a water-based alumina cement (Zircar Alumina Cement) obtained from Zicar Products, Inc. The Zircar Alumina Cement consisted of 70% of alumina in a combination of milled fibers and submicroparticles. It is mildly acidic (pH 5.0) and forms a strong bond on removal of the water solvent. Prior to use, the coated crucibles were first heated at < 100°C in air for 2 h, and then heated to red hot in vacuum at increments of about 200°C for 2 h at each temperature to eliminate the volatiles. This careful programming of heating temperatures also avoided the cracking of the alumina coating. The temperature limit of these crucibles is 1650°C.

Equipment

X-ray powder diffraction (XRD): SCINTAG 3000 XRD diffractometer, SCINTAG;

Transmission electron microscopy (TEM): PHILIPS EM 201 Transmission Electron Microscope;
Mössbauer spectroscopy: Ranger.Scientific Inc. MS-1200 Mössbauer Spectrometer; and
Superconducting quantum interference device (SQUID) magnetometry: MPMS2 SQUID magnetometer.

Preparation of Samples

The SMAD reactor has been described elsewhere *(4,5,13a–c)*. For the evaporation of Fe, Co, and Ni, the crucible was a tungsten basket coated with alumina cement as described above. A fused alumina crucible placed in a tungsten basket was used for the evaporation of the second component, such as MgF_2 or BaF_2. The evaporation followed a similar path as the preparation of bimetallic particles. Prior to the evaporation, the crucibles that contained the metal (such as Fe) and the host material (such as MgF_2) were warmed up to certain ranges of temperatures. This was done by raising the temperatures of the crucibles in increments of about 100°C for a time period of about 2 h. This slow heating process effectively outgassed the starting materials and minimized sudden vaporization surges during deposition. After the crucibles were heated to temperatures about 100–200°C below the boiling points of the starting materials, about 40–50 mL of pentane were deposited on the cold wall of the reactor. Then, with the continuous introduction of pentane vapor, the temperatures of the crucibles were raised slowly until the starting materials began to vaporize. During the whole evaporation process, a constant evaporation of the host material and steady depositions of pentane at rates of about 2–3 mL/p min were ensured before, during, and after the vaporization of the metallic component. After the evaporation, an additional 40–50 mL of pentane was deposited to cover the final product. Then the reactor was closed off from the vacuum line. The liquid nitrogen dewar was removed to allow the reactor to warm up to room temperature. Then, the vacuum was reapplied to remove the pentane, and a black powder was obtained.

After the as-prepared product was transferred into the argon-filled box, heat treatments at various temperatures were applied to these particles to induce phase separation and to increase the sizes of the metal crystallites within these particles. The heat treatments of these particles were carried out with the samples sealed in a Pyrex glass tube or a quartz tube. After the heat treatment, the sample tube was cut open in the dry box, and the particles were stored in a small sample vial and kept in the argon-filled dry box.

The passivation of the surfaces of these materials requires very slow exposure of the particles to air. This was done by keeping the sample in a small sample vial in air for about 24 h with the vial cap slightly loosened. After the heat treatment of the samples, there could still be some

small metal clusters that were not protected by the host material, especially on the surfaces of the particles. The oxidation of these metal clusters would generate a great deal of heat, so if the particles were exposed to air rapidly, the heat generated by the oxidation of the surface metal elements would not only cause the sintering of the particles, but it would also lead to the oxidation of more metal atoms. Therefore, a long period of time is required for the heat to dissipate.

RESULTS AND DISCUSSION

The Fe-MgF_2 System

The evaporation temperature of MgF_2 under the normal SMAD reactor pressure (about 10^{-3} torr) is around 1100°C. The Fe-MgF_2 system studied in this research had a molar ratio of Fe to MgF_2 of 1:2, where about 0.80 g of Fe (14.3 mmol) and 1.78 g MgF_2 (28.6 mmol) were coevaporated and deposited at 77 K with pentane vapor. After the experiment, about 2.0 g of the product could be collected. Figure 1 gives the XRD patterns of the as-prepared, heat-treated, and passivated Fe-MgF_2 (molar ratio 1:2) powders. In the as-prepared sample, signals of MgF_2 and Fe were both present, and the estimated Fe crystallite size was about 9 nm. The XRD patterns of the heat-treated and passivated samples showed only the signals of Fe and MgF_2, and no signals for iron oxides were visible. The estimated XRD sizes of the Fe crystallites for each of the heat treatment temperatures are given in Table 1. A graphic version of the information provided in this table is given in Fig. 2.

Some TEM photos of these particles are shown in Figs. 3 and 4. The TEM measured sizes of the particles and the α-Fe crystallite sizes are listed in Table 2. TEM photos showed that after being heated at lower temperatures, the Fe-MgF_2 particles still had a near single-phase structure with the Fe crystallite embedded in a matrix of MgF_2, and the Fe crystallites did not grow very much. When the temperature reached 500°C, severe phase separation occurred. Most of the Fe clusters aggregated into very large Fe particles (50–100 nm), and only a small number of the smaller Fe crystallites remained. In the 500°C and 600°C samples, there were actually two groups of Fe crystallites. One was the large Fe particles with a size range of around 100 nm, and the other was the remaining smaller Fe crystallites that were about 10–15 nm in size. By visual inspection, we can estimate that the large Fe particles account for more than 90% of the total mass of the Fe in these materials, whereas the small Fe crystallites only represent <10% of the total Fe mass. After the heat treatments at the temperatures of 500 and 600°C, the MgF_2 crystals also grew into large pieces in a size range of a few hundred nanometers.

The magnetic properties of these Fe-MgF_2 particles were studied using a SQUID magnetometer. Although a small portion of the Fe atoms

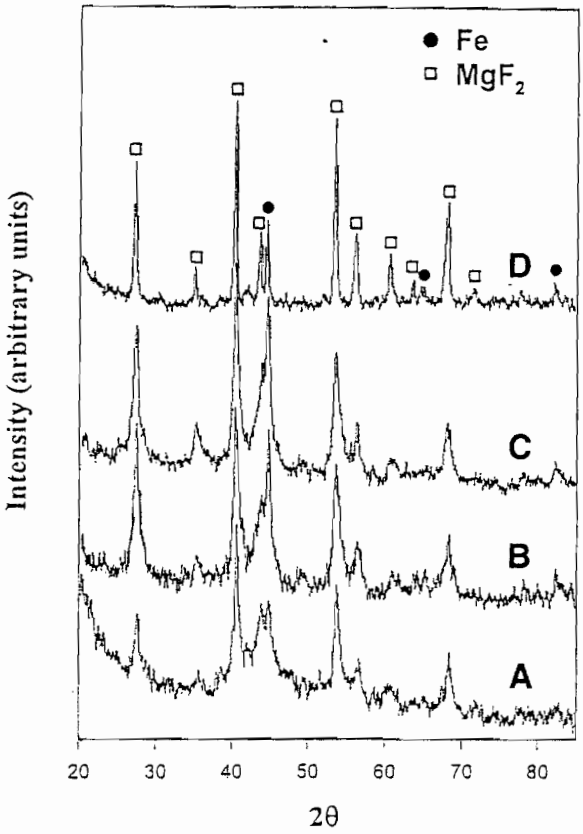

Fig. 1. XRD patterns of fresh and passivated Fe-MgF_2 particles (Fe:MgF_2 = 1:2): **(A)** fresh, as-prepared; **(B)** heat-treated at 200°C and passivated; **(C)** heat-treated at 400°C and passivated; **(D)** heat-treated at 600°C and passivated.

Table 1
XRD Fe Sizes of Fe-MgF_2 Particles Heat-Treated at Different Temperatures

Heat treatment temperature, °C	XRD Fe crystallite size, nm
Room temperature, not heated	9.0
200	12.0
300	15.0
350	18.0
400	22.0
600	60.0

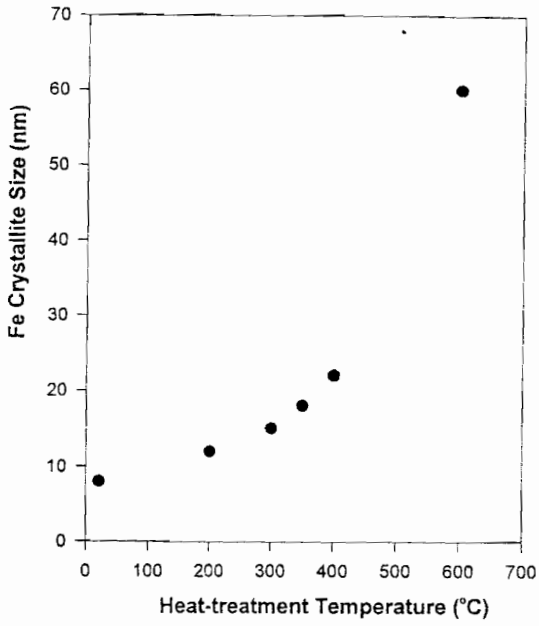

Fig. 2. XRD Fe crystallite sizes of Fe-MgF_2 particles heat-treated at different temperatures.

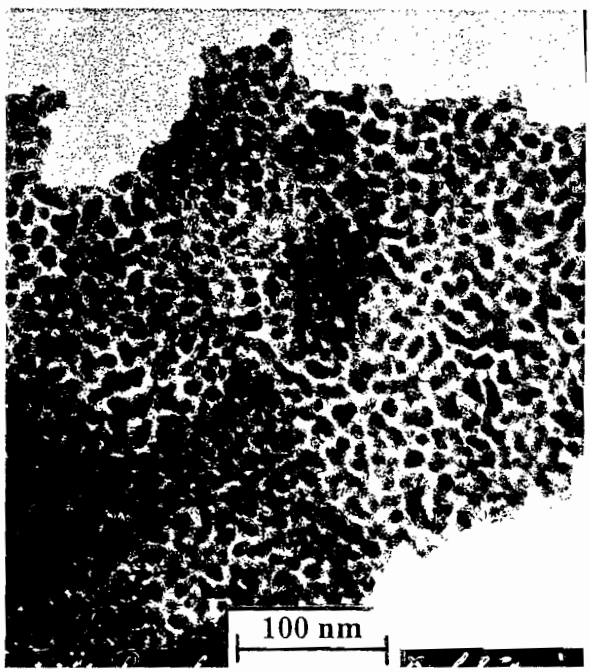

Fig. 3. TEM photo of Fe-MgF_2 particles heat-treated at 200°C for 2 h.

Fig. 4. TEM photo of Fe-MgF_2 particles heat-treated at 500°C for 2 h.

Table 2
TEM Sizes of the Fe-MgF_2 Particles

Heat treatment temperature, °C	TEM overall particle size, nm	TEM α-Fe crystallite, I[a], size, nm	TEM α-Fe crystallite, II[b], size, nm
Room temperature			
200	12–15		
300	17–19		
400	22–25		
500		50–100	10–15
600		50–150	10–15

[a]Large Fe crystallites.
[b]Isolated small Fe crystallites.

in these materials were actually oxidized during the passivation process, the magnetization values per gram of Fe were calculated without consideration of the mass change caused by the oxidation of Fe atoms. This is because the extent of the oxidation was very hard to estimate, and second, the oxidation of Fe should cause only a small change in the mass balance of these materials. The calculated magnetization values of these

Table 3
Magnetization Values of Passivated Fe-MgF_2 Particles

Heat treatment temperature, °C	α-Fe size, nm	Magnetization, emu/g of Fe, at different temperatures, K				
		10 K	77 K	150 K	220 K	300 K
Fresh, as-prepared	9	187	183	177	170	158
200	12	135	134	132	129	125
300	15	203	198	193	185	172
400	22	209	205	200	193	184
600	50–100	219	215	210	205	194

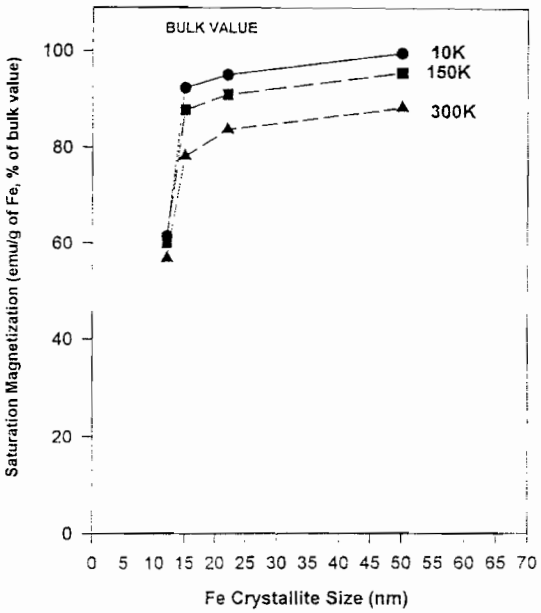

Fig. 5. Saturation magnetization values of the passivated Fe-MgF_2 particles (percentage of Fe bulk value 220 emu/g of Fe).

Fe-MgF_2 materials are listed in Table 3, and the coercivity values are given in Table 4.

Figure 5 gives the percentage of the bulk magnetization value (220 emu/g of Fe) at 300 K vs Fe crystallite sizes in these particles. The magnetization data in Table 3 and the information provided in Fig. 5 show that after being heated at temperatures of 400°C and above, more than 85% of the Fe atoms were protected when these particles were exposed to air. The above results for the Fe-MgF_2 system provide us with enough information to construct a schematic illustration for the formation of

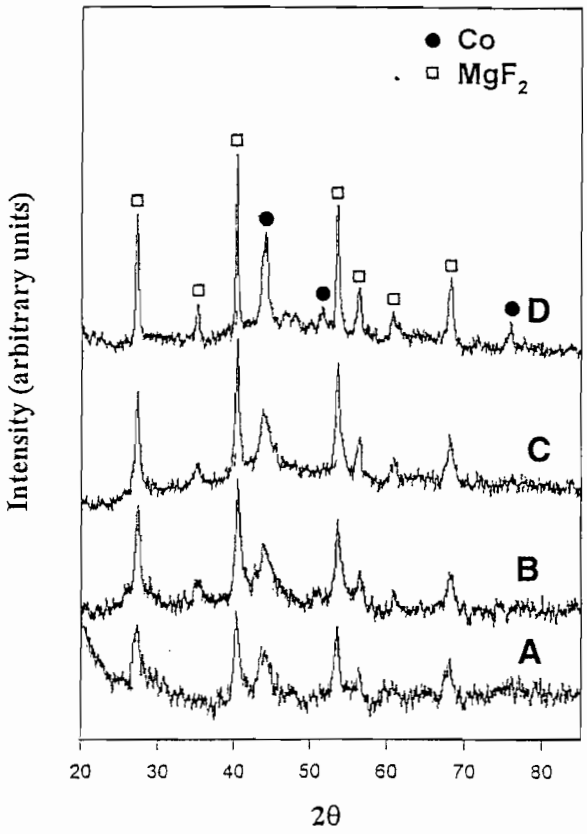

Fig. 6. XRD patterns of fresh and passivated Co-MgF_2 particles: **(A)** fresh, as-prepared; **(B)** heat-treated at 200°C and passivated; **(C)** heat-treated at 400°C and passivated; **(D)** heat-treated at 700°C and passivated.

encapsulated Fe clusters in an MgF_2 matrix with the SMAD method, which was shown in Scheme 1.

The Co-MgF_2 System

The evaporation of Co and MgF_2 followed the same procedure as the evaporation of Fe and MgF_2, Co began to vaporize at about 1300°C under the SMAD reactor pressure. The most studied Co-MgF_2 system had a molar ratio of 1:2 for Co to MgF_2, where about 0.80 g of Co (13.6 mmol) and 1.69 g of MgF_2 (27.2 mmol) were coevaporated. Figure 6 gives the XRD patterns of the fresh, as-prepared Co-MgF_2 powders and the heat-treated and passivated samples. The average size of the Co crystallites of the fresh, as-prepared sample was estimated as approx 4.5 nm by using the Sherrer formula for XRD broadening. All the XRD patterns showed metallic Co and MgF_2 and no clear signals of Co oxides

Table 4
Magnetic Coercivity Values of Fe-MgF_2 Particles

Heat treatment temperature, °C	α-Fe size, nm	Magnetic coercivity, Oe, at different temperatures, K				
		10 K	77 K	150 K	220 K	300 K
Fresh, as-prepared	9	420	270	215	170	105
200	12	955	475	240	179	159
300	15	320	120	120	95	72
400	22	580	370	265	200	130
600	50–100	180	140	90	72	56

Fig. 7. TEM photo of Co-MgF_2 particles heat-treated at 400°C for 2 h.

could be observed. The estimated XRD sizes of Co crystallites in these samples are listed in Table 5, and the estimated TEM Co crystallite sizes are also given if available. Figures 7 and 8 give some TEM photos of these particles.

A graphic version of the heat treatment temperature-Co crystallite size relationship is given in Fig. 9. From the comparison in Table 5 and Fig. 9, we can see that the XRD Co sizes are generally smaller than the

Fig. 8. TEM photo of Co-MgF_2 particles heat-treated at 600°C for 2 h.

sizes estimated from the TEM photos. This is because in the XRD patterns of the Co-MgF_2 particles, the Co line ($2\theta = 44.2°$) by which the Co crystallite sizes were calculated with the Scherrer formula partially overlaps with an MgF_2 line that is at about 39.8° of 2θ. As a result, the calculated XRD Co sizes are actually smaller than they should be, and the TEM sizes should be more trustworthy. The properties of these Co-MgF_2 particles are listed in Tables 5–7, and also shown in Figs. 10 and 11.

Since Co has a bulk magnetization value of 162.5 emu/g of Co, from Table 6 and Fig. 10 we can see that at least 80% of the Co atoms were protected if these particles were heated at temperatures higher than 500°C before they were exposed to air. The Co-MgF_2 system has a much narrower Co size distribution. A more simplified schematic illustration can be given for the encapsulation of Co particles in the MgF_2 (Scheme 2).

The Ni-MgF_2 System

The evaporation of Ni and MgF_2 also followed the same procedures as the evaporation of Fe and MgF_2; Ni began to vaporize at about 1400°C under the SMAD pressure. The most studied Ni-MgF_2 system had a molar ratio of 1:2 for Ni to MgF_2, where about 0.80 g of Ni (13.6 mmol) and 1.69 g of MgF_2 (27.2 mmol) were coevaporated in the presence of pen-

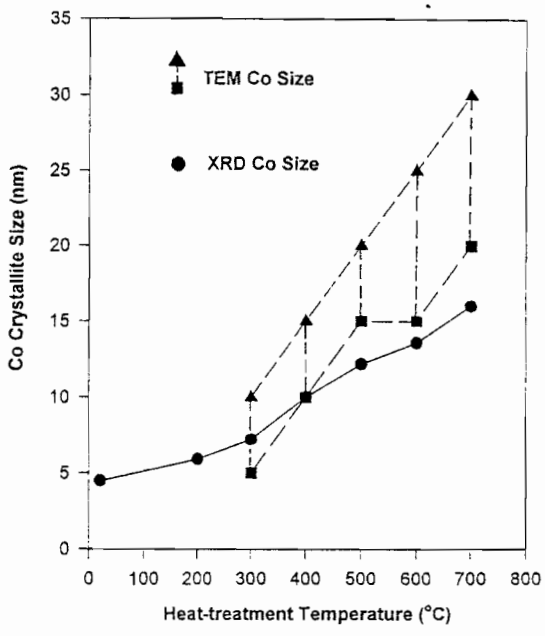

Fig. 9. Co crystallite sizes of Co-MgF_2 particles heat-treated at different temperatures.

Table 5
Estimated Co Crystallite Sizes in the Co-MgF_2 Particles

Heat-treatment temperature, °C	XRD Co crystallite size, nm	TEM Co particle size, nm
Fresh, as-prepared	4.5	
200	5.9	
300	7.2	5–10
400	10.0	10–15
500	12.2	15–20
600	13.6	15–25
700	16.0	20–30

tane. Figure 12 gives the XRD patterns of the fresh, as-prepared, and the heat-treated and passivated Ni-MgF_2 particles. The average sizes of the Ni crystallites were estimated as about 5.8 nm in the fresh, as-prepared sample. In all the XRD patterns of the heat-treated and passivated samples, only the signals of Ni and MgF_2 were clearly visible, whereas no signs of Ni oxides could be detected. Some of the TEM photos of these particles are given in Fig. 13. The estimated XRD sizes and TEM sizes of the Ni crystallites are listed in Table 8.

Table 6
Saturation Magnetization Values of Co-MgF_2 Particles

Heat treatment temperature, °C	XRD Co size, nm	TEM Co size, nm	Saturation magnetization values, emu/g of Co, at different temperatures, K				
			10 K	77 K	150 K	220 K	300 K
Fresh, as-prepared	4.5		113	111	109	107	106
200	5.9		102	101	100	99	98
300	7.2	5–10	105	104	103	101	100
400	10.0	10–15	107	104	103	101	100
500	12.2	15–20	120	118	117	116	115
600	13.6	15–25	131	129	129	128	128
700	16.0	20–30	134	132	131	131	130

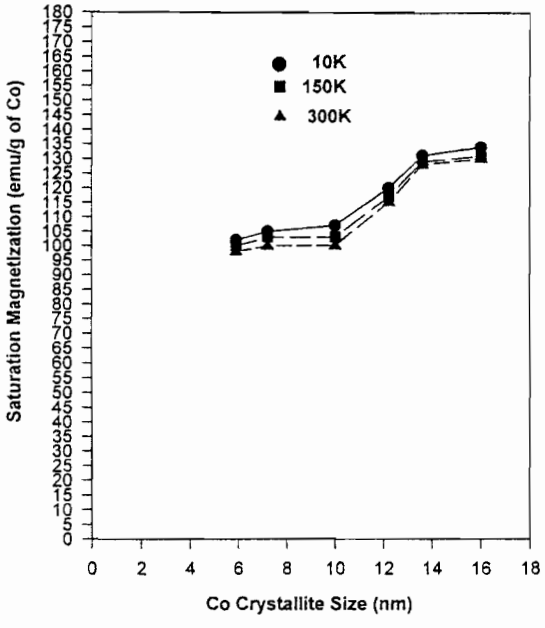

Fig. 10. Saturation magnetization values of passivated Co-MgF_2 particles with different Co sizes (XRD size).

From the above comparison, we can see that the XRD and TEM sizes agree with each other very well. The magnetic properties of these materials are listed in Tables 9 and 10. Figures 14 and 15 also illustrate some of these results.

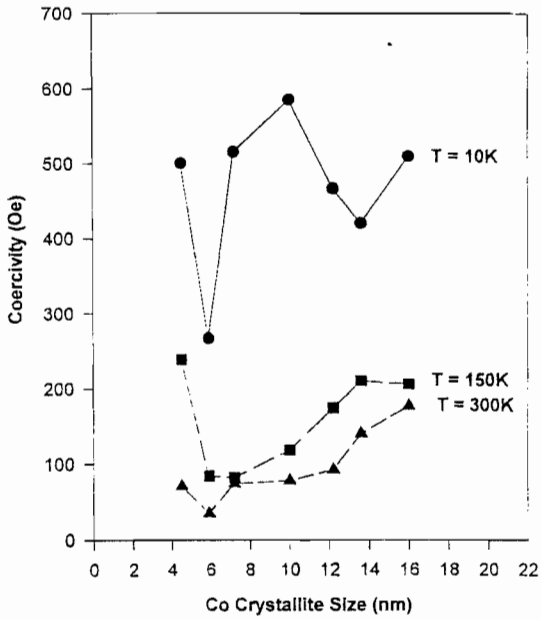

Fig. 11. Magnetic coercivity values of passivated Co-MgF_2 particles at different temperatures.

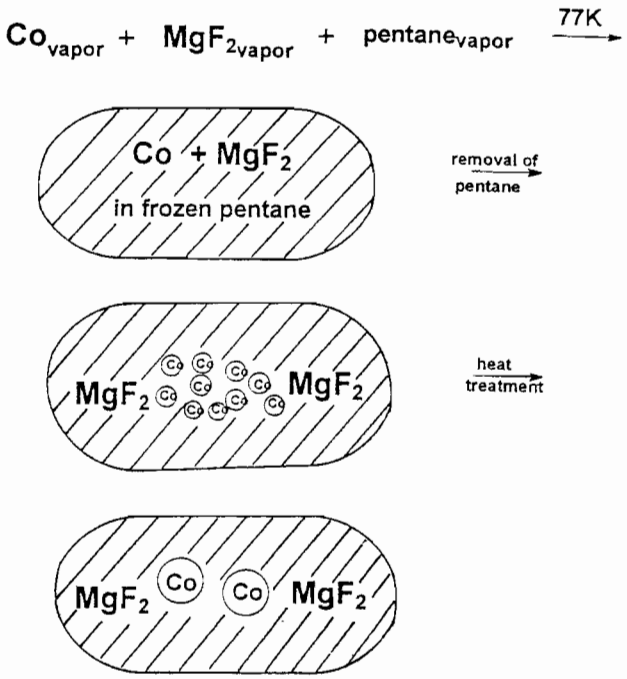

Scheme 2. Encapsulation of Co clusters in MgF_2.

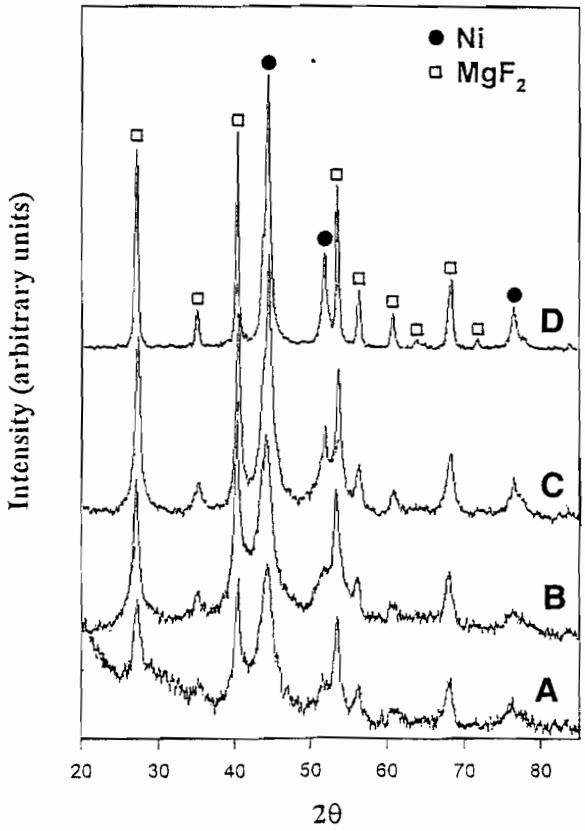

Fig. 12. XRD patterns of fresh and passivated Ni-MgF_2 particles: **(A)** fresh, as-prepared; **(B)** heat-treated at 200°C and passivated; **(C)** heat-treated at 400°C and passivated; **(D)** heat-treated at 600°C and passivated.

The Fe-BaF_2 System

BaF_2 sublimes at 700° C under the pressure of 10^{-4} torr. The Fe-BaF_2 system studied in this research had a molar ratio of 1:1 for Fe to BaF_2 particles, only the signals of BaF_2 were visible. In the XRD pattern of passivated sample that had been heated at 400° C for 2 h, still no signs of metallic Fe could be detected. After the Fe-BaF_2 sample was heated at 600°C, it began to show visible signs of metallic Fe in its XRD pattern. The size of the Fe particles became very large at this point. The magnetic studies of this sample in air showed very disappointing results. Only about 8.0% of the bulk value was achieved. It is reasonable to believe that a large portion of the Fe atoms in this sample were oxidized when it was exposed to air. However, the Fe-BaF_2 system should still be of some interest in the study of encapsulated small magnetic particles. At first, it may

Fig. 13. TEM photo of Ni-MgF_2 particles heat-treated at 500°C for 2 h.

Table 7
Magnetic Coercivity Values of Co-MgF_2 Particles

Heat treatment temperature, °C	XRD Co size, nm	TEM Co size, nm	Coercivity values, Oe, at different temperatures, K		
			10 K	150 K	300 K
Fresh, as-prepared	4.5		500	239	71
200	5.9		267	84	35
300	7.2	5–10	515	82	74
400	10.0	10–15	585	118	78
500	12.2	15–20	466	174	92
600	13.6	15–25	420	210	140
700	16.0	20–30	509	206	177

Table 8
XRD and TEM Sizes of Ni Crystallites in the Ni-MgF_2 Particles

Heat treatment temperature, °C	XRD Ni crystallite size, nm	TEM Ni crystallite size, nm
Fresh, as-prepared	5.8	
200	7.5	7
300	8.5	5–10
400	11.0	10
500	13.6	10–15
600	19.0	15–25

formed. MgF_2 was found to be a very good protecting agent against the oxidation of the small metal crystallites when these materials were exposed to air. The MgF_2 encapsulated Fe, Co, and Ni particles obtained after heat treatments at high temperatures (above 500°C) had saturation magnetization values very close to their bulk values. For samples heated at lower temperatures, reduced saturation magnetization values were observed when they were exposed to air. Although metal oxides (such as α-Fe_2O_3) may be present in some of the passivated samples, the formation of metal oxides may not account for all of the saturation magnetization reduction with crystallite size. The study of completely oxygen-free materials is necessary to reveal the effect of oxidation on the magnetic properties of these materials, and these studies are under way.

ACKNOWLEDGMENT

The financial support of the National Science Foundation is acknowledged with gratitude.

REFERENCES

1. Sharrock, M. P., *MRS Bull.* **XV(3),** 53 (1990).
2. Sharrock, M. P., *IEEE Trans. Magn.* **26(1),** 193 (1990).
3. Leslie-Pelecky, D. L. and Rieke, R. D., *Chem. Mater.* **8,** 1770 (1996).
4. Glavee, G. N., Kernizan, C. F., Klabunde, K. J., Sorensen, C. M., and Hadijpanayis, G. C. *Chem. Mater.* **3,** 967 (1991).
5. Klabunde, K. J., Zhang, D., Glavee, G. N., Sorensen, C. M., and Hadijipanayis, G. C. *Chem. Mater.* **6,** 784 (1994).
6. Zhang, D., Glavee, G. N., Klabunde, K. J., Sorensen, C. M., and Hadjipanayis, G. C. *High Temp. Mater. Sci. in press.*
7. Chien, C. L. in *Science and Technology of Nanostructured Materials* (Hadijpanayis, G. C. and Prinz G. A., eds.), Plenum, New York, pp. 477–496 (1991).
8. Papaefthymiou, V., Tsoukatos, A., Hadjipanayis, G. C., Simpoulous, A., and Kostikas, A., *J. Magn. Magn. Mater.* 140–144, 397 (1995).
9. Giri, A. K., de Julián, C., and Gonzaléz, J. M., *J. Appl. Phys.* **76(10),** 6573 (1994).
10. Dormann, J. L., Sella, C., Renaudin, P., and Gibart, P., *Thin Solid Films,* **5,** 983 (1979).
11. Yoshizaki, F., Tanaka, N., and Mihaam, K. Z., *Phys. D—Atoms, Molecules and Clusters,* **19,** 259 (1991).
12. Cowen, J. A., Tsai, K. L., and Dye, J. L., *J. Appl. Phys.* **76,** 6567 (1994).
13a. Klabunde, K. J., Efner, H. F., Murdock, T. O., and Ropple, R., *J. Am. Chem. Soc.* **98,** 1021 (1979).
13b. Klabunde, K. J., *Free Atoms, Clusters, and Nanoscale Particles,* Academic, San Diego, CA (1994).
13c. Klabunde, K. J., and Cardenas-Trivino, G., in *Active Metals—Preparation, Characterization, Applications* (Fürstner, A., ed.), VCH, Weinheim, 1996, p. 237 (1996).